minerals

MDPI

Article

Proterozoic Deep Carbon—Characterisation, Origin and the Role of Fluids during High-Grade Metamorphism of Graphite (Lofoten–Vesterålen Complex, Norway)

Ane K. Engvik [1,*], Håvard Gautneb [1], Pål Tore Mørkved [2], Janja Knežević Solberg [1] and Muriel Erambert [3]

[1] Geological Survey of Norway, P.O. Box 6315 Torgarden, N-7491 Trondheim, Norway; havard.gautneb@ngu.no (H.G.); janja.knezevic@ngu.no (J.K.S.)
[2] Department of Earth Science, University of Bergen, P.O. Box 7803, N-5020 Bergen, Norway; pal.morkved@uib.no
[3] Department of Geosciences, University of Oslo, P.O. Box 1047, N-0316 Oslo, Norway; m.m.l.erambert@geo.uio.no
* Correspondence: ane.engvik@ngu.no (A.K.E.); Tel.: +47-73904000 (A.K.E.)

Abstract: Graphite formation in the deep crust during granulite facies metamorphism is documented in the Proterozoic gneisses of the Lofoten–Vesterålen Complex, northern Norway. Graphite schist is hosted in banded gneisses dominated by orthopyroxene-bearing quartzofeldspathic gneiss, including marble, calcsilicate rocks and amphibolite. The schist has major graphite (<modality 39%), quartz, plagioclase, pyroxenes, biotite (Mg# = 0.67–0.91; Ti < 0.66 a.p.f.u.) and K-feldspar/perthite. Pyroxene is orthopyroxene ($En_{69–74}$) and/or clinopyroxene ($En_{33–53}Fs_{1–14}Wo_{44–53}$); graphite occurs in assemblage with metamorphic orthopyroxene. Phase diagram modelling (plagioclase + orthopyroxene (Mg#-ratio = 0.74) + biotite + quartz + rutile + ilmenite + graphite-assemblage) constrains pressure-temperature conditions of 810–835 °C and 0.73–0.77 GPa; Zr-in-rutile thermometry 726–854 °C. COH fluids stabilise graphite and orthopyroxene; the high Mg#-ratio of biotite and pyroxenes, and apatite Cl < 2 a.p.f.u., indicate the importance of fluids during metamorphism. Stable isotopic $\delta^{13}C_{graphite}$ in the graphite schist is −38 to −17‰; $\delta^{13}C_{calcite}$ of marbles +3‰ to +10‰. Samples with both graphite and calcite present give lighter values for $\delta^{13}C_{calcite}$ = −8.7‰ to −9.5‰ and heavier values for $\delta^{13}C_{graphite}$ = −11.5‰ to −8.9‰. $\delta^{18}O_{calcite}$ for marble shows lighter values, ranging from −15.4‰ to −7.5‰. We interpret the graphite origin as organic carbon accumulated in sediments, while isotopic exchange between graphite and calcite reflects metamorphic and hydrothermal re-equilibration.

Keywords: C-isotope; fluid; granulite; graphite; Vesterålen

Citation: Engvik, A.K.; Gautneb, H.; Mørkved, P.T.; Solberg, J.K.; Erambert, M. Proterozoic Deep Carbon—Characterisation, Origin and the Role of Fluids during High-Grade Metamorphism of Graphite (Lofoten–Vesterålen Complex, Norway). *Minerals* **2023**, *13*, 1279. https://doi.org/10.3390/min13101279

Academic Editor: José Francisco Molina Palma

Received: 16 August 2023
Revised: 22 September 2023
Accepted: 23 September 2023
Published: 29 September 2023

1. Introduction

Graphite, a mineral composed of pure C, forms during the higher-grade metamorphism of sediment rich in organic matter [1,2], by reaction and deposition from COH-rich fluids in granulite [3] or igneous terranes [4]. Graphite in Precambrian crustal rocks has been reported worldwide, including in Sri Lanka [5], India [6], Mozambique [7], Madagascar [8] and Greenland [9]. In Scandinavia, graphite is a common mineral in Early Proterozoic terranes and occurs widely in the 2.0 Ga Svecokarelian of Sweden and Finland [10–12], the Paleoproterozoic crust of north Norway and Finland [13–17] and the Sveconorwegian Bamble lithotectonic domain of south Norway [18]. Strauss et al. [19] showed that the enrichment of carbonaceous material occurred worldwide at 2.0–2.4 Ga, but with a particular clustering on the Fennoscandian shield.

Graphite, which shows a "flake" or a high-ordered structure in metamorphic rocks, is usually described in arenites and metapelites. Touret [18] and Newton et al. [20] argued that a massive CO_2 flux through the lower crust is required for the formation of anhydrous orthopyroxene-bearing granulite formation. Lamb and Valley [21] pointed out the importance of fO_2 buffering by the rock, stating that fO_2 estimates in many terranes are so low

that graphite should precipitate. However, the lack of graphite observations in orthopyroxene granulites has led to a continuing discussion. The relevance of the CO_2-flushing process for granulitisation and graphite precipitation has been discussed from a plate tectonic perspective (e.g., [22–24]). Meanwhile, the presence and importance of graphite [6,24] and its deposition during volatile processes [3,4,25] have been debated. Case et al. [2] described the metamorphic effect on the formation of graphite deposits. Stable C isotopes of graphite have been used to investigate the carbon origin of graphite formation [26–28]. Viewed against this background, our documentation of graphite coexisting with orthopyroxene is relevant for the long-term discussion of the formation of graphite in granulite.

In this study, we use field data, drill core logging, petrography, mineral chemistry, petrology and stable C isotopes to document graphite formation and reworking in the Proterozoic orthopyroxene-bearing granulite facies gneisses of Lofoten–Vesterålen Complex in northern Norway (Figure 1). From the stable C isotopes, we interpret the graphite origin to be the organic carbon accumulated in sediments related to the Early Proterozoic global Lomagundi–Jatuli isotopic excursion. From the petrography and mineral chemistry, we establish the reaction equations, producing and consuming fluids stabilising graphite with orthopyroxene. Graphite P-T stability under granulite facies conditions is calculated using the thermometers Zr-in-rutile, the graphite–calcite isotopic Δ^{13}C-ratio and pseudosection modelling. The results are used to discuss the origin of deep Proterozoic carbon, the petrogenetic processes of graphite re-equilibration in granulite and the role of fluids.

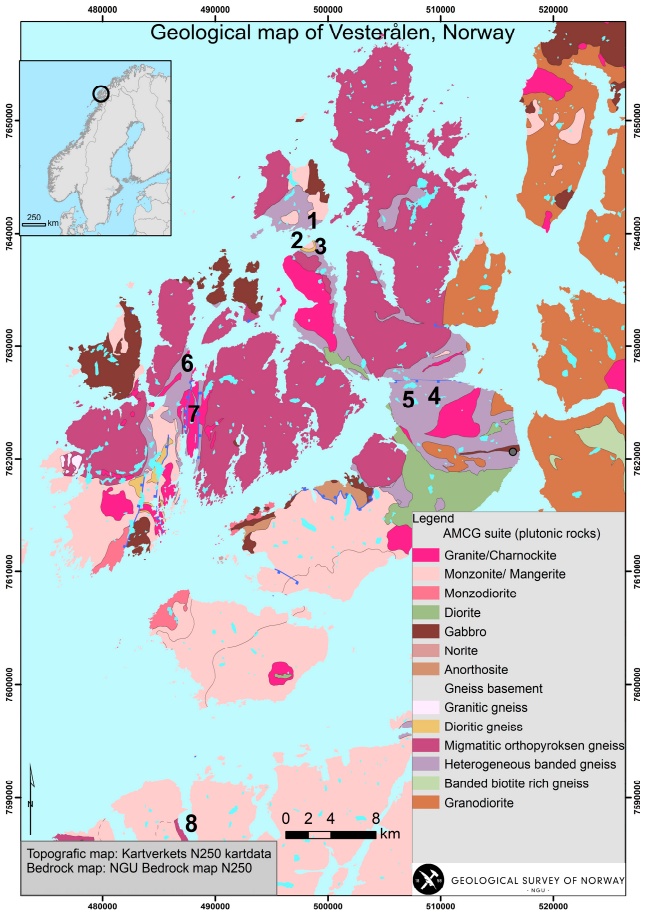

Figure 1. Geological map of Vesterålen, north Norway. Main sampled graphite localities are numbered.

Geological Setting

The study area, which is part of the Lofoten–Vesterålen Complex of northern Norway, is an Archaean to Early Proterozoic gneiss basement intruded by a magmatic anorthosite–mangerite–charnockite–granite (AMCG) suite (Figure 1; [29,30]). U-Pb geochronology con-

firmed the presence of Archaean to Early Proterozoic rocks [31–33], while the AMCG suite was emplaced into the basement at 1870–1790 Ma [34]. The oldest gneisses are preserved as granodioritic granitic and orthopyroxene-bearing migmatites with a crustal formation age dating back to c. 2650 Ma [32]. The granulite facies crustal basement of the Lofoten–Vesterålen Complex, including orthopyroxene granitoids and gneisses, covers an area of more than 2000 km^2 [29]. Markl et al. [35] described anorthosites, mangerites and charnockites of the AMCG suite of Lofoten that intrude at 0.4 GPa and 800–925 °C. Sequences of graphite-bearing heterogenous banded gneisses are dominated by orthopyroxene-bearing gneiss, interlayered with quartzite, amphibolite, graphite schist and marble.

Graphite was first reported in Vesterålen by Keilhau [36], and deposits were mined in 1899–1914 and 1949–1960. Modern investigations of the graphite deposits in the area are summarised by Gautneb and Tveten [13] and Gautneb et al. [15,16]. Baker and Fallick [37,38] investigated stable isotopes of marble and associated graphite connecting the signatures to a metamorphic fluid influx while Palosaari, Latonen, Smått, Blomqvist and Eklund [14] studied the quality of the graphite by using XRD and Raman spectroscopy.

From 2013 to 2019, the graphite-bearing provinces of northern Norway were explored for new graphite deposits with economical potential. The work found inferred aggregated graphite resources of 241 Mt ore with an average graphite content of 11.6% [15,16].

2. Materials and Methods

2.1. Petrological Investigations

Geological field investigation, extensive sampling, drill core logging and the definition of graphite content, quality and resource estimation were reviewed by Rønning et al. [39] and Gautneb et al. [15,16]. To understand the petrological processes causing the graphite deposition, a selected sample set (Supplementary Table S1) was investigated for this study.

The polished thin sections were studied using optical microscopy and scanning electron microscopy (SEM) using a LEO 1450 VP instrument situated at the Geological Survey of Norway (NGU). Semi-quantitative X-ray mineral identification was carried out using an energy-dispersive spectrometer mounted on the SEM.

Mineral chemistry (Tables S2–S8), used for petrological interpretations and modelling, was analysed using a Cameca SX100 electron microprobe equipped with 5 wavelength-dispersive spectrometers (WDS) at the Department of Geosciences, University of Oslo. The accelerating voltage was 15 kV, the beam current was 15 nA and the counting time at the peak was 10 s. A focused electron beam was used for pyroxene, scapolite and garnet, and a beam diameter of 5 to 10 µm for plagioclase, biotite and apatite. The calibration was performed using a selection of synthetic and natural minerals and oxides. The matrix corrections were carried out by the PAP program [40]. Zr-in-rutile (Table 1) was analysed with an accelerating voltage of 20 kV, a beam current of 100 nA, a beam diameter of 2 µm and a counting time at the peak of 180 s. The calibration standard for Zr was Monastery Mine zircon and the accuracy of the method was checked by analysing the rutile standard R10 [41].

Equilibrium assemblage diagrams were calculated using Theriak-Domino [42], and the internally consistent thermodynamic dataset of [43]. The mineral activity models are those of Holland and Powell [44] and Baldwin et al. [45] for feldspar, White et al. [46] for biotite, orthopyroxene, ilmenite and liquid, and Holland and Powll [47] and Green et al. [48] for clinopyroxene. Bulk rock composition is derived from major element XRF and TOC analyses (Tables S9 and S10). H_2O concentrations are based on the "loss on ignition" (LOI) analysis subtracted by measured C content. The calculations were run assuming H_2O activity of 0.5. The calculations were performed in the MnNCKFMASH-TCO (MnO-Na_2O-CaO-K_2O-FeO-MgO-Al_2O_3-SiO_2-H_2O-CO_2-TiO_2) system.

2.2. Whole Rock Chemistry, Total Carbon (TC), Total Organic Carbon (TOC) and Total Sulphur (TS)

The whole rock chemistry on an extensive sample set of graphite schist in Vesterålen has been reported by Rønning et al. [39,49] and Gautneb et al. [15,50]. The whole rock

element analyses were conducted at NGU and measured on fused glass beads prepared by 1:7 dilution with lithium tetraborate. The samples were analysed on a PANalytical Axios XRF spectrometer equipped with a 4 kW Rh X-ray end-window tube, using common international standards for calibration. The whole rock major element analyses used for pseudosection modelling are presented in Supplementary Table S9.

The reported contents of total carbon (TC), total organic carbon (TOC) and total sulphur (TS) were analysed using a Leco SC-632 analyser. The detection limits were 0.06%, 0.1% and 0.02% for TC, TOC and TS, respectively. The analytical uncertainty at the 2 σ level was ±15%, ±20% and ±30%, respectively. TC and TOC used for pseudosection modelling are presented in Supplementary Table S10.

A Niton XL2 portable XRF was used for bulk rock chemical reconnaissance along the drill core, with 4 point measurements per metre down the core.

2.3. Stable Isotopes

C and O isotopic compositions of graphite and calcite (Table 2) were analysed from whole rock sample powder, and the presence of graphite versus calcite was verified by the TC and TOC results. Graphite-bearing samples for carbon isotope analyses were dried (60 °C) and homogenised before being weighed into tin capsules for analysis. Samples that contained both calcite and graphite were homogenised and dried as above, and split for C and O isotope analyses of calcite and C isotope analyses of graphite. To the latter part, 3 M HCl was added and left until the visible reaction stopped. The sample was washed and 3 M HCl was added again and left to react overnight to remove all carbonates. The samples were then repeatedly washed with DI water until near neutrality, dried (at 60 °C) and weighed. This method is the basis for reporting isotopic values for graphitic carbon ($\delta^{13}C_{graphite}$) in graphite schist and $\delta^{18}O_{calcite}$ values along with $\delta^{13}C_{calcite}$ values for carbonate carbon from marble samples (Table 2).

The graphite carbon isotopes were measured on a Thermo Scientific Flash EA 1112 connected to a Delta V Plus isotope ratio mass spectrometer, which was calibrated to meet international standards USGS24, IAEA-600 and IAEA-CH6. The calcite was measured on a Thermo Scientific Kiel IV connected to a MAT 253 dual inlet isotope ratio mass spectrometer, which was calibrated with two marble house standards that were calibrated to meet IAEA standards and the international standard NBS-18. All international standards were distributed by IAEA. External reproducibility (1σ) was always better than 0.08‰ for the calcite analyses. Repeated analyses of graphite $\delta^{13}C$ were 0.25‰ or better. Values are given in ‰ relative to VPDB (Vienna Pee Dee Belemnite) for both C and O.

3. Results

3.1. Field Relations

The graphite-rich zones in Vesterålen follow the banded gneiss sequence (Figure 1), where the graphite is concentrated in graphite schist within massive pyroxene-bearing quartzofeldspathic gneiss. The graphite-bearing units are poorly exposed, and the regional pattern of the graphite zones was determined by geophysical EM mapping [39,51,52]. Based on combined EM measurements and field mapping, the graphite-rich zones were found to have thicknesses from <1 m to 200 m. They appear in large-scale foliation-parallel subvertical structures extending for several km along the strike, and as individual en echelon graphite lenses.

At shoreline exposures, the enriched graphite zones outcrop as dark-grey well-foliated schist (Figure 2). A strong schistosity causes the graphite zones to crumble easily (Figure 2a,b). At the best-exposed outcrop on the small island of Svinøy (Locality 2; Figure 2a,b,d), the foliation trend of the graphite schist can be followed northwards to the locality Skogsøy (Locality 1; Figure 2b,c,e) and southward to the locality Smines (Locality 3). An enrichment of graphite in the schist causes a lustrous rock colour (Figure 2f).

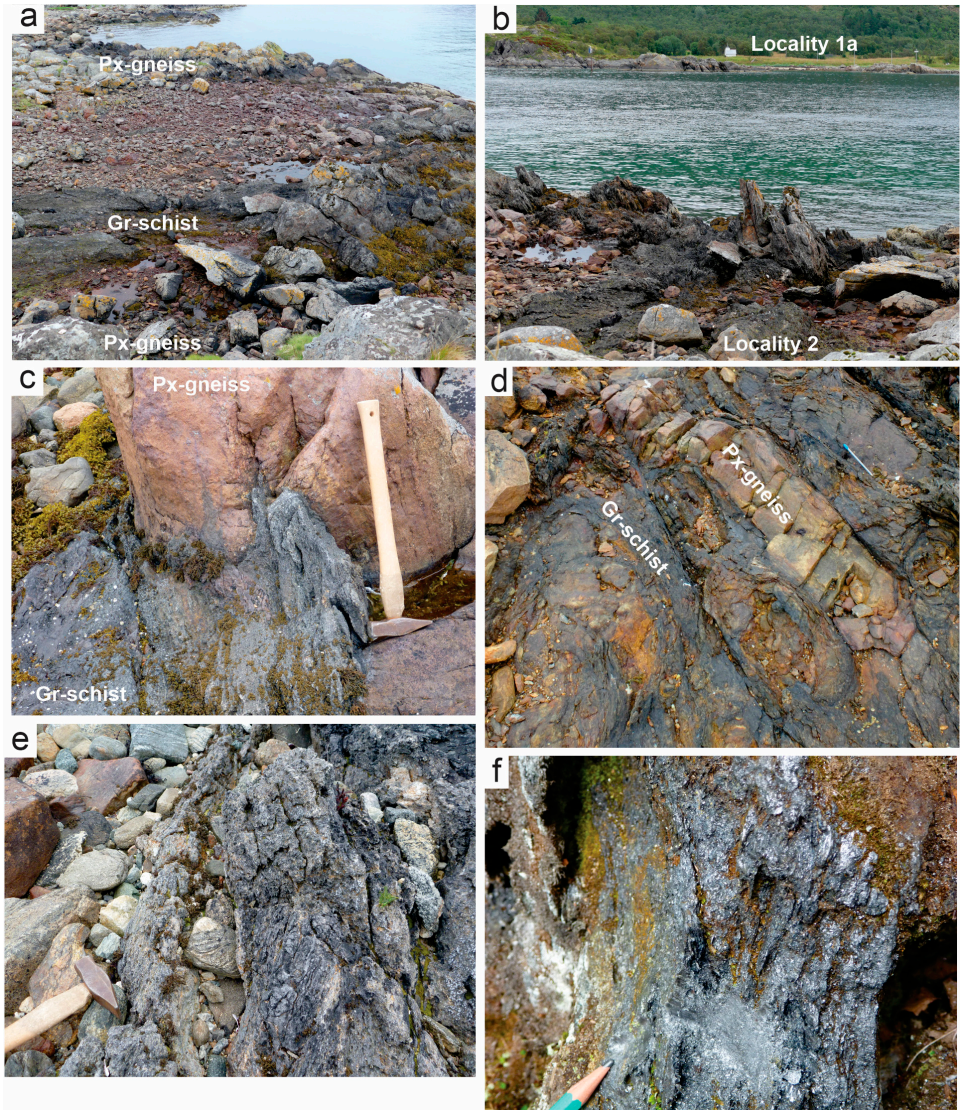

Figure 2. Field pictures of graphite schist and host rock (abbreviations after Whitney and Evans [53]). (**a**) A c. 10 m thick zone of graphite schist in pyroxene gneiss. The locality illustrates the easily crumbled nature of the graphite, which causes few and poor exposures of this rock. Svinøy (Loc. 2). (**b**) Strongly foliated and schistose graphite schist at Svinøy (Loc. 2). The direction of foliation illustrates that the graphite schist horizon continues under the sea and is exposed again at the shoreline of Skogsøy (Loc. 1) across the fjord. (**c**) Strongly foliated and schistose dark-grey graphite schist in contact with massive pyroxene gneiss. The rusty colour of the gneiss indicates a high content of sulphide. Skogsøy (Loc. 1). (**d**) A 15 cm thick rusty pyroxene gneiss lens included in the graphite schist, Svinøy (Loc. 2). (**e**) Dark-grey graphite schist, easily crumbling at the shoreline locality of Skogsøy (Loc. 1). (**f**) Graphite schist at Hornvatn (Loc. 5). The enrichment in graphite causes the lustrous colour of the rock.

There is a pronounced lithological contrast between massive host gneisses and the graphite schist (Figure 2c). The host pyroxene gneiss has a pale brownish colour, is massive and locally stromatic, and in the vicinity of graphite schist occurs with a characteristically rusty colour. Small lenses of host rock can occur internally in the graphite schist (Figure 2d).

Graphite-rich zones are sometimes associated with horizons of marbles and calcsilicate rocks, as for the Golia locality (Locality 4), Hornvatn (Locality 5) and Sommarland (Locality 7; Figure 3), and are locally intruded by charnockite, or with horizons of amphibolite (Table S1).

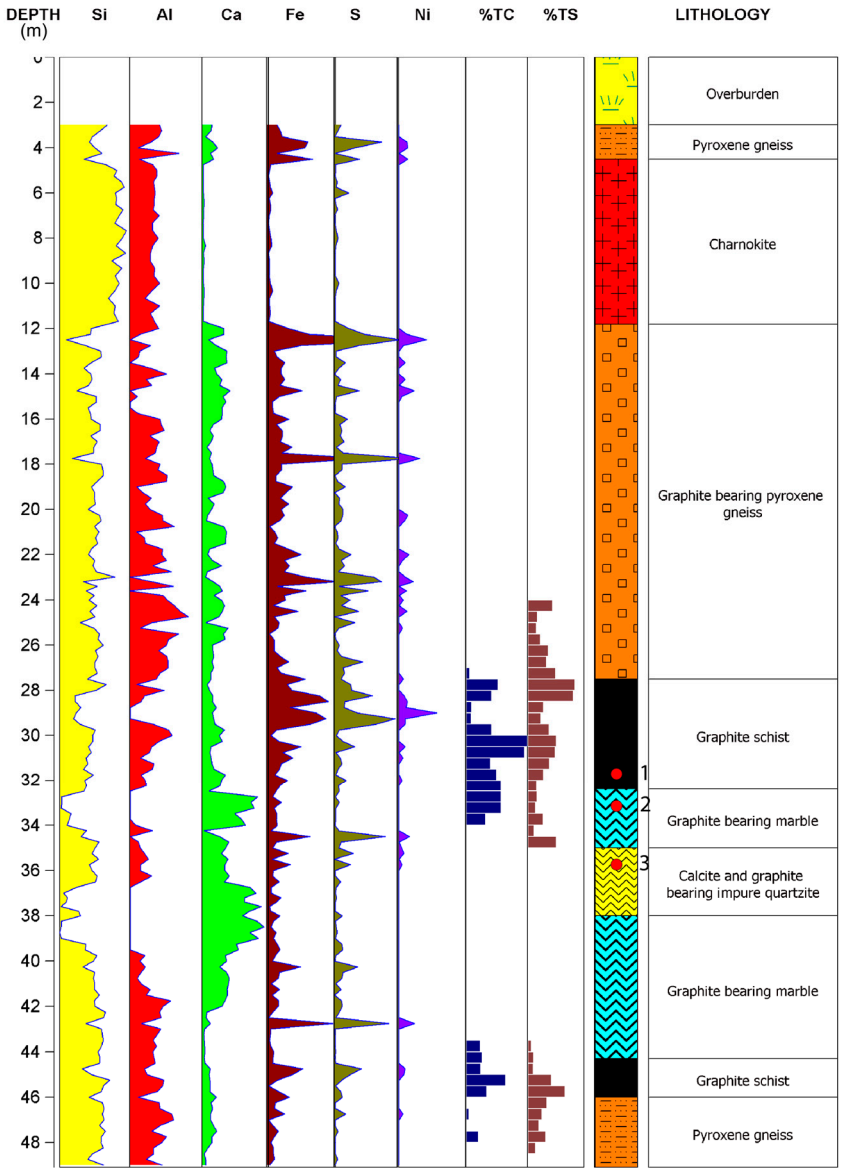

Figure 3. Drill core (Sommarland, Loc. 7) showing the typical setting of the graphite schist with close approximation to pyroxene gneisses, impure marbles and calcsilicates. Elemental variation is measured with a portable XRF and total carbon and sulphur by Leco analyser (see [39] for raw data). Red dots indicate the sample point of samples 1–3 in Table 3.

Several drill cores from the Vesterålen graphite deposits are described by Gautneb et al. and Rønning et al. [50,54] and Gautneb et al. [15]. The drill core log in Figure 3 presents a typical setting for the graphite schist from Locality 7, Sommarland at Langøya, and is regarded as representative. The drill core loggings confirm the graphite schist's close relationships to the pyroxene gneiss, exemplifying a graphite schist in contact with a marble bench, including graphite-bearing marble and calcite- and graphite-bearing impure quartzite. Carbonate horizons are locally present, and the charnockite dykes cut the graphite-bearing units. The drill core logging also illustrates that disseminated graphite is present tens of metres deep into the host pyroxene gneisses.

Integrated with the drill core logging (Figure 3), bulk chemical data measured by portable XRF illustrates the strong heterogeneity of the schist in the graphite-bearing gneiss sequence. Leco analyses run through the graphite schist and host rock shows the strong relationships between logged graphite schist and graphite-bearing marble with high TC and TS. In addition to the chemical data presented in the drill core logs, whole rock

chemistry and TC, TOC and TS analyses are presented in Gautneb et al. and Rønning et al. [15,39,50,54].

3.2. Petrography and Mineral Chemistry

Graphite schist characteristically has a major content of graphite (Table S1; Figure 4a–c) varying up to a modality of 39%, with a measured average of TC = 15%, a maximum of 44% and median of 12%, but with small-scale variations [39]. Quartz and plagioclase ($Ab_{47–93}An_{5–52}$) are additional major phases, together with pyroxenes, biotite and K-feldspar ($Ab_{1–8}Kfs_{92–99}$) or perthite ($Ab_{35–64}An_3Kfs_{50–62}$) (Figure 5a–d). Pyroxene is present either as orthopyroxene ($En_{69–74}Fs_{26–29}$; Mg# = 0.70–0.74), clinopyroxene ($En_{33–53}Fs_{1–14}Wo_{44–53}$; Mg# = 0.70–0.97), or both (S1), and generally shows high Mg# in the graphite schist (Figure 5a,b). Biotite is usually phlogopite with a high Mg# = 0.80–0.91 and Ti content up to 0.66 a.p.f.u., although Mg# locally decreases to 0.67 (S3; Figure 5c). The highest Mg# of biotite is measured in graphite schist of Sommarland (<0.91; Loc. 7), Møkland (<0.88; Loc. 6), Mofjord (<0.83; Loc. 8) and Svinøy (<0.91; Loc. 2). Locally occurring amphibole is edenite or pargasite with Mg# = 0.87–0.92 and Ti = 0.10–0.14 a.p.f.u. (S4). Ti phases are present as titanite and rutile. The graphite schist is often sulphide-rich, with pyrite, pyrrhotite and local chalcopyrite. Apatite is common and shows variable amounts of Cl up to 2 a.p.f.u. and F up to 1.44 a.p.f.u. (Figure 5d). The localities of Møkland and Sommarland show the highest concentrations of Cl in apatite, while apatite in the graphite schist of Smines (Locality 3) has the highest F content (Table S8).

Graphite occurs as euhedral high-ordered flake graphite, with a heterogeneous grain size from fine to coarse. Graphite schist with high graphite concentrations shows a characteristic dissemination of coarse and fine flakes (Figure 4a,b). Graphite has a crystal-preferred orientation contributing to the well-developed foliation and schistosity of the rock, together with crystal-preferred oriented biotite (Figure 4c–e). In assemblage with graphite, the pyroxenes, quartz and feldspars constitute anhedral matrix minerals with metamorphic triple-point grain boundaries, and are normally fine- to medium-grained (Figure 4a–e).

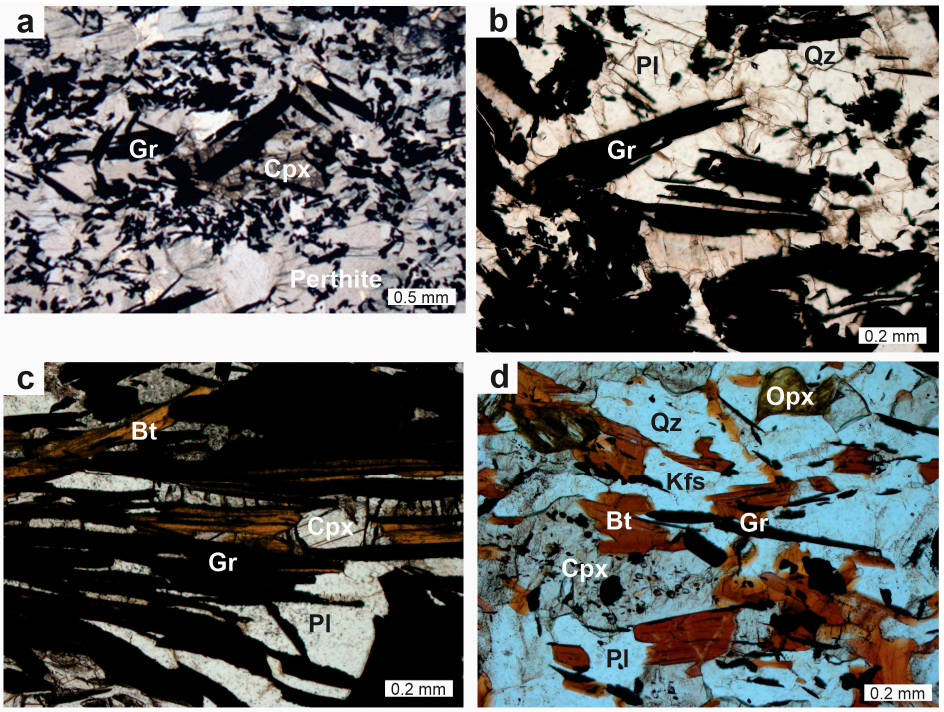

Figure 4. *Cont.*

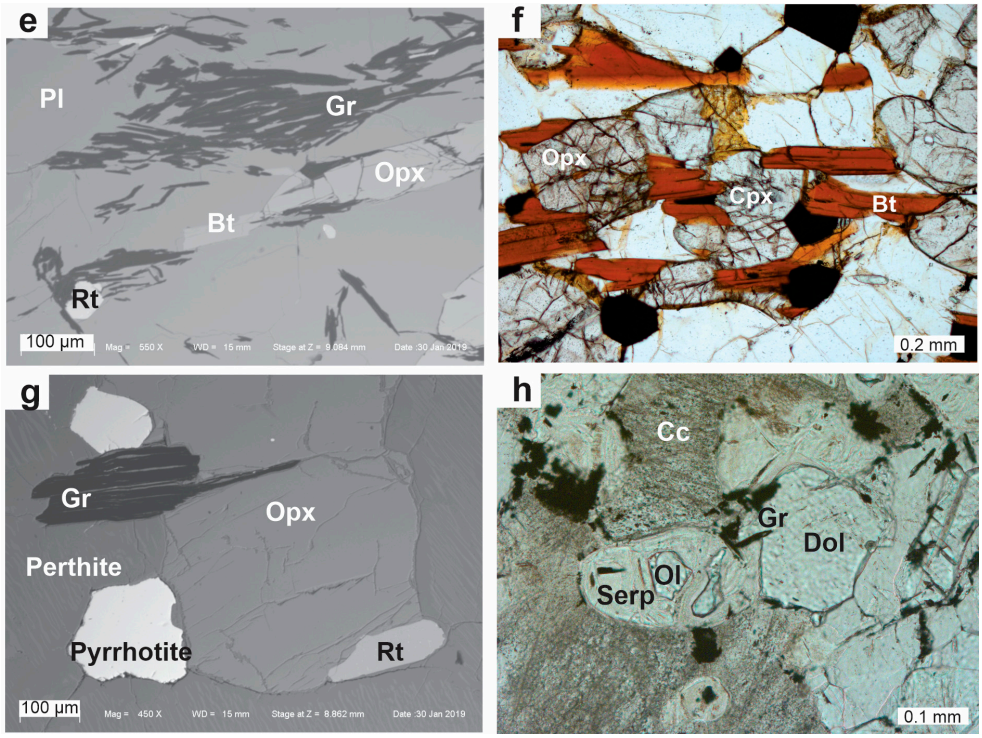

Figure 4. Photomicrographs (plane light) and BSE-images from graphite schist and host rocks (abbreviations after Whitney and Evans [53]). (**a**) Heterogranular graphite schist with high concentrations of medium- and fine-grained flake graphite in matrix with perthite and clinopyroxene. Photomicrograph, sample VAE34, Sommarland (Locality 7). (**b**) Well-developed crystals of flake graphite in graphite schist, together with quartz and plagioclase. Photomicrograph, sample VAE149, Skogsøy (Loc. 1). (**c**) Strongly foliated graphite schist with high concentrations of graphite with matrix phases biotite, plagioclase and clinopyroxene. The strong foliation is defined by crystal-preferred orientation (CPO) graphite and biotite, and shape-preferred orientation (SPO) clinopyroxene. Photomicrograph, sample VAE171, Hornvatn (Loc. 5). (**d**) Graphite with orthopyroxene, clinopyroxene, biotite, quartz and feldspars in graphite schist. The sample show a weaker foliation defined by CPO biotite and graphite and SPO clinopyroxene. Additional opaque phases are pyrrhotite and minor chalcopyrite. Photomicrograph, sample VAE163, Smines (Loc. 3). (**e**) High concentrations of graphite in equilibrium with orthopyroxene, biotite, plagioclase and rutile. Foliation is defined by CPO graphite and biotite and SPO orthopyroxene. BSE image, sample VAE161, Svinøy (Loc. 2). (**f**) Host pyroxene gneiss with orthopyroxene, clinopyroxene and biotite. The opaque phases are pyrrhotite and chalcopyrite. A weaker foliation is defined by CPO biotite. Photomicrograph, sample VAE151, Skogsøy (Loc. 1). (**g**) Graphite in host pyroxene gneiss. The BSE image illustrates the equilibration of graphite with orthopyroxene, perthite, rutile and pyrrhotite. Sample VAE164, Smines (Loc. 3). (**h**) Dolomite–calcite marble with olivine (partly reacted with serpentine) with some disseminated very fine-grained graphite. Photomicrograph, sample VAE167, Golia (Loc. 4).

In addition to the main graphite schist assemblage described above, a few localities show additional major phases of scapolite and epidote. The scapolite is a major phase in the graphite schist of Sommarland drill core 1702, but is also present in drill core 1701 (Table S1). The scapolite is $Me_{74–81}$ with a variable Cl content up to 0.17 a.p.f.u., but is low in S (Table S7). At Møkland (Locality 6), scapolite is present as corona on sulphide, as $Me_{36–37}$ showing S = 0.05–0.07 a.p.f.u. and with a high Cl of 0.66 a.p.f.u. (Table S6).

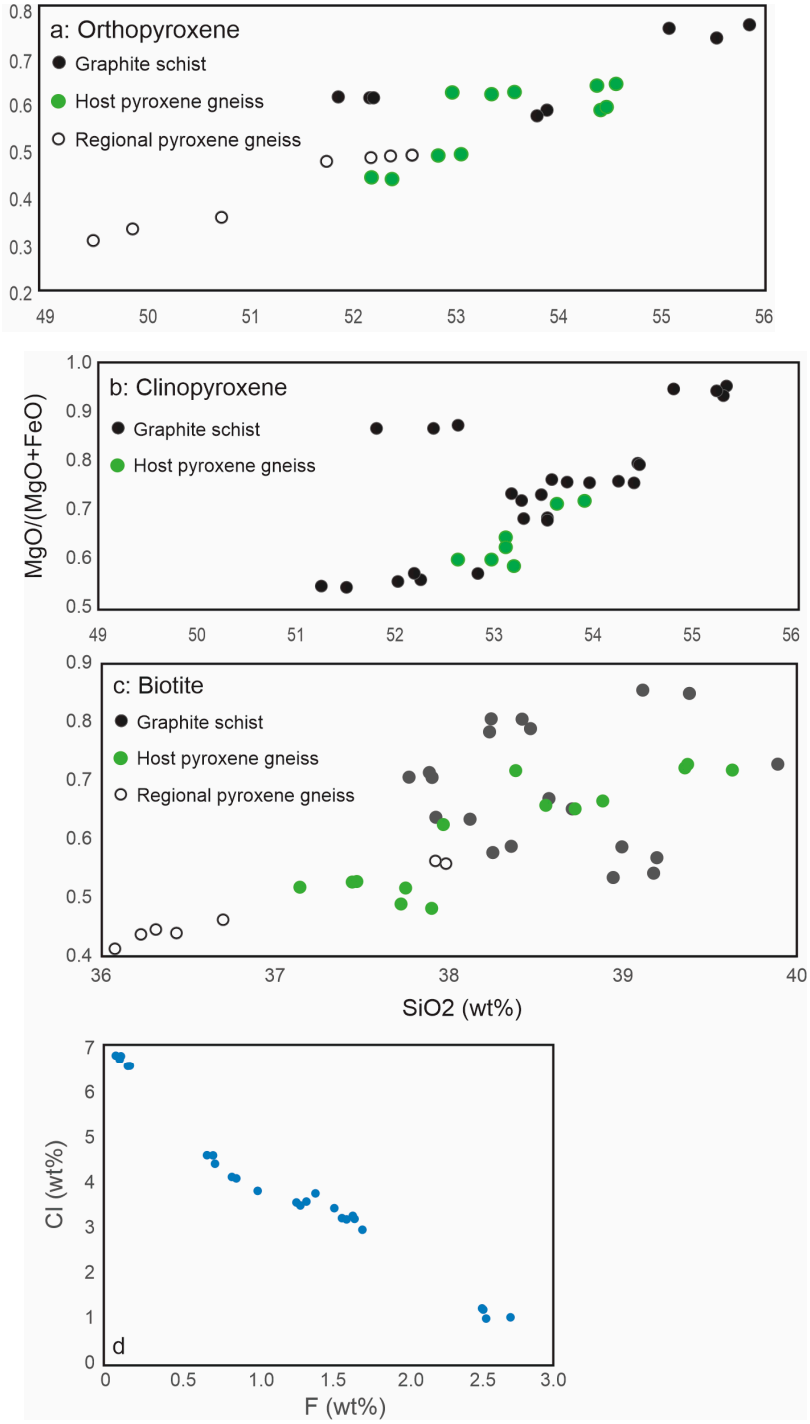

Figure 5. Chemistry plots of minerals from graphite schist. (**a**) MgO/(MgO + FeO)-SiO_2 in orthopyroxene. (**b**) MgO/(MgO + FeO)-SiO_2 in clinopyroxene. (**c**) MgO/(MgO + FeO)-SiO_2 in biotite. (**d**) Cl-F content in apatite.

The southernmost graphite deposit of Mofjord (Locality 8) also differs in mineralogy with the presence of clinozoisite, white mica and minor garnet. The clinozoisite is present as coarse porphyroblast up to several centimetres in size. The heterogranular white mica is muscovite with Si = 6.5–6.6 a.p.f.u. and Mg < 0.82 a.p.f.u. (Table S3). Very fine-grained euhedral garnet is spessartine $Alm_{16}Prp_{47–48}Grs_5Sps_{31–32}$ (Table S5).

Orthopyroxene gneiss constitutes a major part of the mapped heterogenous banded gneiss sequence (Figure 1) and hosts the graphite schist. The orthopyroxene gneiss has major plagioclase ($Ab_{48–83}An_{16–50}$), perthite ($An_{0–1}Ab_{8–13}Kfs_{87–92}$) or K-feldspar, quartz

and orthopyroxene ($En_{57–75}Fs_{24–42}$). Locally, clinopyroxene ($En_{39–44}Fs_{9–17}Wo_{40–47}$) and biotite (Ti = 0.69–0.76 a.p.f.u) are present (Figure 5). The Mg# of the mafic phases is variable but relatively high; orthopyroxene shows Mg# = 0.58–0.76, clinopyroxene Mg# = 0.72–0.83 and biotite Mg# = 0.63–0.66 (Tables S2 and S4; Figure 5a–c). Graphite is an accessory and is in equilibrium with orthopyroxene, as shown by their joint grain boundaries (Figure 4g). In addition, accessory assemblages of ilmenite, Fe oxide, rutile, apatite, zircon and pyrrhotite may be present.

The gneiss is equigranular, fine- to medium-grained, with a metamorphic triple-point grain boundary texture. The texture is normally granoblastic but with a modal banding and shows a locally weak preferred orientation of biotite (Figure 4f). The transition from enriched graphite schist to pyroxene gneiss, although sharp in outcrops with respect to schistosity and strain, is petrographically and mineralogically gradual. Pyroxene gneiss shows a variable but increased graphite content towards graphite schist zones. The transition zone often has a rusty colour, which can be explained by a high sulphide content as pyrite, pyrrhotite and minor chalcopyrite (Figure 4g).

Marble and calcsilicate rock horizons are locally associated with graphite schist and are documented at Golia (Locality 4), Hornvatn (Locality 5) and Sommarland (Locality 7; drill core 1701; Figure 3). The marbles vary between calcite–dolomite marble and horizons richer in silicate minerals. Calcite–dolomite marble shows a variable content of olivine ($Fo_{97–98}$) partly replaced with serpentine (Figure 4h), local clinopyroxene ($En_{48–50}Wo_{50–52}$), and spinel, Mg-bearing ilmenite, zircon and apatite and local graphite as an accessory. The marble has a fine- to medium-grained equigranular and granoblastic texture, where olivine/serpentine aggregate and clinopyroxene occur as rounded minerals within the carbonate matrix. Silicate minerals include phlogopite (Mg# = 0.97, Ti = 0.32 a.p.f.u.), clinopyroxene ($En_{15–18}Fs_{30–33}Wo_{52–53}$), olivine/serpentine ($Fo_{95}$), K-feldspar ($Ab_{6–8}Kfs_{92–94}$) and quartz. Graphite occurs locally. The accessory minerals are titanite, spinel, apatite, pyrrhotite, chalcopyrite and Fe oxide.

Amphibolite occurs locally, layered in the banded complex hosting graphite schist and may include disseminated graphite. The amphibolite is granoblastic medium-grained with major plagioclase ($An_{33–35}$), orthopyroxene ($En_{86–87}Fs_{12–14}$), amphibole and biotite. Orthopyroxene has a high Mg# = 0.86–0.88, and biotite has a high Mg# = 0.88 and Ti of 0.35–0.36 a.p.f.u. Amphibole is pargasite with Mg# = 0.89 and Ti = 0.2 a.p.f.u. The disseminated graphite occurs as flake graphite. Accessory apatite is Cl- and F-rich with Cl < 1.33 and F < 0.55 a.p.f.u. Other accessories are dominantly sulphides, such as pyrite, pyrrothite and chalcopyrite. Cl-rich scapolite ($Me_{36–37}$) with Cl = 0.65–0.66 and S = 0.05–0.07 is found as corona between plagioclase and sulphide.

3.3. Petrology

3.3.1. Pressure–Temperature Pseudosection Modelling

Pseudosection modelling was run to define the pressure–temperature condition and the phase stability fields of the graphite-bearing rocks. The presented pseudosection was calculated for the P-T window of 0.6–0.9 GPa and 750–850 °C. Figure 6 is a representative pseudosection for graphite schist (sample VAE161, Locality 2 Svinøy). The calculation shows stability for the observed equilibrium assemblage of plagioclase + orthopyroxene + biotite + quartz + rutile + ilmenite + graphite at temperatures between 795 and 845 °C and pressures up to 0.85 GPa. Orthopyroxene is stable at temperatures above 780 °C, while biotite breaks down at T above 830 °C. Rutile is present throughout the calculated P-T interval, together with ilmenite, which shows the same stability as expected for the higher P-T end. Isopleths for the Mg# ratio of orthopyroxene (Table S2) were used to better constrain P-T conditions; the measured Mg# ratio = 0.74 indicates a stability field of 810–835 °C at 0.73–0.77 GPa for the graphite- and orthopyroxene-bearing gneiss.

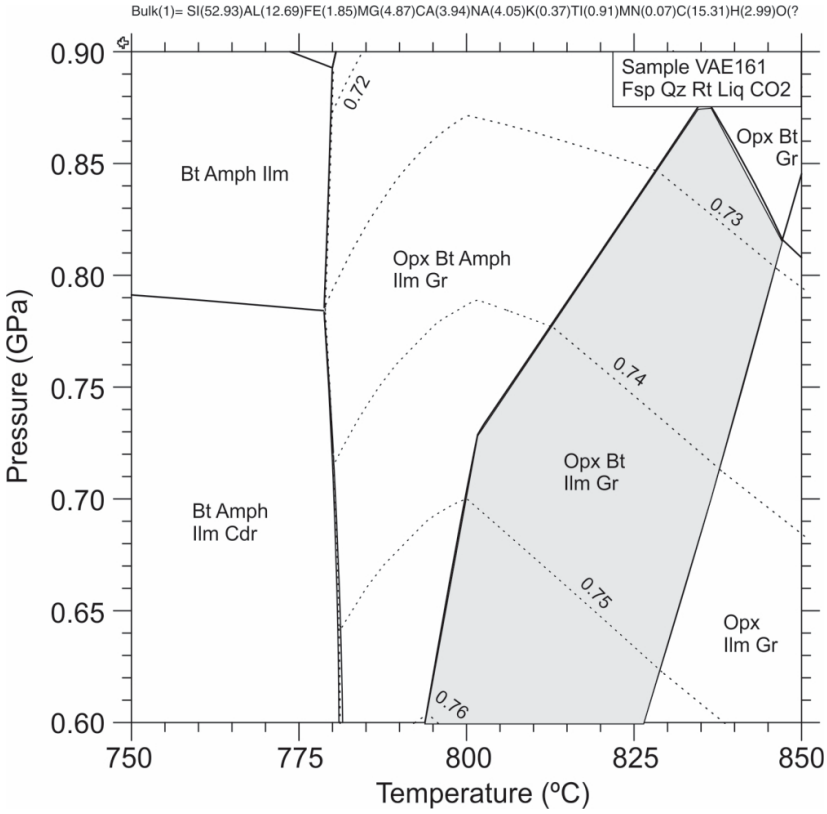

Figure 6. P-T pseudosections (sample VAE161; graphite-orthopyroxene-bearing schist; Svinøy, Locality 2), calculated by Theriak-Domino. The diagram illustrates phase stability fields with respect to P and T. The grey-shaded area represents the stability of the observed assemblage. Stippled lines are isopleths representing the orthopyroxene Mg# ratio. See text for discussion.

3.3.2. Zr-in-Rutile Thermometry

Additional thermometric calculations were based on the Zr content in rutile using the different calibrations by Kohn, Tomkins et al. and Watson et al. [55–57]. The calculations use an average of individual analyses in specific rutile crystals (see Table 1), assuming P = 0.75 GPa (7.5 kbar) in accordance with the result from the above P-T pseudosection modelling. Depending on the calibration, the Zr-in-rutile results spread from 726 to 751 °C for the graphite schist sample VAE159, and between 774 and 854 °C for the orthopyroxene host rock gneiss (samples VAE164, BH1BØ4-60). The T estimates are in accordance with the T indicated by the pseudosection modelling, although showing some spread in T.

Table 1. Zr-in-rutile thermometry.

Locality	Rock Type	Sample No.	Analyse	Zr ppm	P (kbar)	T (°C)	T (°C)	T (°C)
					(assumed)	(57)	(56)	(55)
Svinøy	Graphite schist	VAE159	#18-19-20	991	7.5	751	742	737
(Loc. 2)			#21-23	893	7.5	741	732	726
Smines	Opx-gneis	VAE164	#13	1855	7.5	819	806	813
(Loc. 3)	(host rock)		#11-13-19	1369	7.5	785	774	775
Møkland	Opx-gneis	BH1BØ4-60	#7-10	2476	7.5	854	838	851
(Loc. 6)	(host rock)		#9	2046	7.5	831	817	825

Detection limit 66 ppm. Standard deviation (2σ) 40–47 ppm. Standardisation made on Monastery Mine zircon.

3.4. Carbon and Oxygen Isotopes

$\delta^{13}C$ values are reported for graphitic carbon in graphite schist (Table 2) and $\delta^{18}O$ values along with $\delta^{13}C$ values for carbonate carbon from marble samples. Two of the marble

samples were from benches in contact with graphite schist (sample VAE167, Locality 4, Golia; sample VAE172, Locality 5, Hornvatn). Three samples contained mixed graphite and calcite (SOM1701-59; SOM1701-60; SOM1701-61, Locality 7, Sommarland; Figure 3), and the paired carbonate–graphite isotope data are reported.

Table 2. Carbon and oxygen isotope composition of graphite schists and marble (numbers 1–3 refer to Figure 3 with indicated sample locations).

Sample	Rock Type	δ13C/δ12C$_{VPDB}$ Graphite	δ13C/δ12C$_{VPDB}$ Calcite	δ18O/δ16O$_{VPDB}$	Δ^{13}C Calcite and Graphite
SOM1701-59 AV **(1)**	Graphite schist/marble	−11.50	−9.52	−15.40	1.98
SOM1701-60 AV **(2)**	Graphite schist/marble	−10.26	−8.63	−15.29	1.63
SOM1701-61 AV **(3)**	Graphite schist/calc silicate	−8.88	−8.56	−15.59	0.32
SOM1702-25 AV	Graphite schist	−30.18			
VAE146	Graphite schist	−27.97			
VAE147	Graphite schist	−28.01			
VAE159	Graphite schist	−30.41			
VAE161	Graphite schist	−32.02			
VAE163	Graphite schist	−29.77			
VAE165	Graphite schist	−38.67			
VAE166B	Graphite schist	−24.01			
VAE171	Graphite schist	−21.01			
BH1BØ30.10	Graphite schist	−17.52			
VAE206	Graphite schist	−28.89			
VAE231	Graphite schist	−23.19			
VAE232	Graphite schist	−23.91			
VAE120	Marble		9.42	−9.56	
VAE118	Marble		10.38	−7.53	
VAE221	Marble		9.95	−9.93	
VAE222	Marble		10.04	−9.96	
VAE167	Marble *		6.14	−13.60	
VAE172	Marble *		3.53	−15.44	
VAE141	Marble		10.27	−9.81	
VAE143C	Marble		9.81	−8.82	
VAE178	Marble		8.14	−13.70	
VAE176	Marble		6.45	−13.45	
VAE235	Marble		9.09	−11.17	
VAE239	Marble		10.30	−9.25	

* the two samples VAE167 and VAE172 in the lightest end of −15.4‰ to −13.6‰.

Most of the graphite schist shows a variation in $\delta^{13}C_{graphite}$ values from −38 to −17‰, with a mean $\delta^{13}C_{graphite}$ value of −27.4‰. The $\delta^{13}C_{calcite}$ values of marbles range from about +3‰ to about +10‰ with an average $\delta^{13}C_{calcite}$ of +8.6‰. For the two marble samples occurring in the vicinity of graphite schist (VAE167 and VAE172), the $\delta^{13}C_{calcite}$ is in the

lighter end of this range, being +6.1‰ and +3.5‰, respectively. The isotopic composition of the mixed graphitic and calcite carbon ($\delta^{13}C_{calcite}$ and $\delta^{13}C_{graphite}$) gives lighter values for the calcite ($\delta^{13}C_{calcite}$ = −8.7‰ to −9.5‰) and heavier values for graphite compared to the "pure" samples ($\delta^{13}C_{graphite}$ = −11.5‰ to −8.9‰).

$\delta^{18}O_{calcite}$ for marble shows relatively light values for calcite ranging from −15.4‰ to −7.5‰, and the two samples VAE167 and VAE172 are at the lightest end of −15.4‰ to −13.6‰. The $\delta^{18}O_{calcite}$ of mixed graphite and calcite samples is also in the light range, from −15.6‰ to −15.3‰.

The degree of isotopic equilibrium between carbonate and graphitic carbon has been shown to be useful as a thermometer in high-grade metamorphic rocks. Our $\delta^{13}C_{calcite}$ and $\delta^{13}C_{graphite}$ pairs show a difference ($\Delta^{13}C$) of 1.98, 1.63 and 0.32, respectively (samples som1701-59, 60 and 61; Table 3). We calculated the equilibrium temperature using the approach of Dunn and Valley [58] and Wada and Suzuki [59]. Two out of three pairs yielded reasonable temperature estimates, yielding temperatures ranging from 850 to 900 °C. One pair, however, that showed a very small $\Delta^{13}C$ (0.32), yielded a very high, likely unrealistic apparent temperature (1130–1156 °C), representing calcite and graphite grains that did not acquire isotopic equilibrium, or that were disturbed during later metamorphic events.

Table 3. Calculated temperatures (°C) based on differences in $\delta^{13}C$ in calcite and graphite ($\Delta^{13}C$) using the thermometers by Wada and Suzuki [59] (W&S) and Dunn and Valley [58] (D&V).

Sample	$\Delta^{13}C$	W&S (°C)	D&V (°C)
som1701-59 AV	1.98	852	847
som1701-60 AV	1.63	901	893
som1701-61 AV	0.32	1156	1129

4. Discussion

4.1. Origin of C and Metamorphic Formation of High-Ordered Graphite

Apart from a brief mention in Baker and Fallick [37,38], the carbon isotope composition of graphite in the investigated area has not yet been reported. In general, a light composition of graphite ($\delta^{13}C_{graphite}$, around −25‰) indicates organic deposited carbon (e.g., [4]). $\delta^{13}C_{graphite}$ values in our graphite schists from Vesterålen range from −38 to −17‰ and are consistent with the typical variation for Archean and Proterozoic organic matter (e.g., [60–63]).

For the calcite in marbles, the unusually heavy $\delta^{13}C_{calcite}$ of +3‰ to about +10‰ (average of +8.6‰) of the Vesterålen marbles, also noted by Baker and Fallick [37], has later been explained by their formation during the global Lomagundi–Jatuli isotopic excursion, which in Fennoscandia was age-constrained to the 2.20–2.06 Ga interval (e.g., [62,64,65]), when such isotopically anomalous carbonates accumulated. Assuming this is correct, this means that the organic matter is the source rock for the Vesterålen graphite mineralisation deposited contemporaneously with the Shungite in Russian Karelia [15,19,66].

A reworking of carbon can cause a shift from $\delta^{13}C$ to heavier composition, although it is relatively resistant to resetting. The present graphite mineralisation in Vesterålen occurring as disseminated graphite or as concentrations in graphite schist in the granulite basement still show relatively light values, but the granulitisation may explain the spread of the data up to −17‰ (Table 2). The later metamorphism, forming the high-grade graphite mineralisation, occurred alternatively during the reported Early Proterozoic event [32,67] or during the emplacement of the AMCG suite at 1870–1790 Ma [31].

The notably heavier $\delta^{13}C_{graphite}$ composition of the mixed graphite and calcite in samples SOM1701-59, SOM1701-60 and SOM1701-61 of −11.5 to −8.9 is explained by an exchange of isotopes between the graphite and calcite during metamorphism, also resulting in the markedly lighter $\delta^{13}C_{calcite}$ of −9.5 to −8.6.

$\delta^{18}O_{calcite}$ will more easily be disturbed by an alteration shifting towards lighter signatures. The $\delta^{18}O_{calcite}$ of the marbles in our studied samples of Vesterålen is relatively

light, ranging from −15.4‰ to −7.5‰, and possibly reflects metamorphic and hydrothermal processes.

4.2. Granulite Facies Metamorphic Formation of High-Ordered Graphite

Our petrographic investigations illustrate the high-ordered structure of graphite in the Vesterålen complex (Figure 4). The crystallographic and mineralogical properties, including the Raman spectroscopy of graphite from other study areas, were well documented by Palosaari, Latonen, Smått, Blomqvist and Eklund [14], who studied the quality of the graphite from the Golia-Hornvatnet area (our localities 4–5, Figure 1). By using XRD and Raman spectroscopy, Palosaari, Latonen, Smått, Blomqvist and Eklund [14] found that the spacing of the (002) reflection was in the range of 0.335–0.336 nm, and G and 2D bands were present at c. 1579 cm^{-1} and c. 1350 cm^{-1}, respectively, documenting the well-developed crystallisation and full ordering of the graphite [68,69] 2016). Rantitsch, Lämmerer, Fisslthaler, Mitsche and Kaltenböck [69] included Raman spectroscopy data from the adjacent Skaland graphite deposit, with a similar geological setting to the present research area [16] and references therein, and showed that the graphite from Skaland is also fully ordered. Based on the Raman measurements, Palosaari, Latonen, Smått, Blomqvist and Eklund [14] determined the temperature of graphite formation to be 575–620 °C. This is lower than our estimated temperatures based on PT pseudosection, Zr-in rutile measurement and isotopic equilibrium. The thermometer based on Raman spectroscopy is sensitive to the measuring procedures [70] and has a restricted temperature range, particularly with respect to high temperature, and the peak T conditions in the graphite-bearing rocks of the Vesterålen complex are by all probability near the upper limit or above what is applicable for Raman spectroscopy, even when using the extended temperature intervals presented by Ratitisch and Linner [71].

In this study, we document the metamorphic graphite equilibrated with orthopyroxene (Figure 4e,g). Although graphite usually occurs in quartzitic and metapelitic rocks, or as vein deposits in the granulite facies crust, descriptions of graphite–orthopyroxene stability are few [6,72]. Pseudosection modelling of graphite–orthopyroxene paragenesis (plagioclase + orthopyroxene; Mg#-ratio = 0.74 + biotite + quartz + rutile + ilmenite + graphite) constrains its stability field to pressure–temperature conditions of 810–835 °C and 0.73–0.77 GPa (Figure 6), in accordance with granulite facies stability. Zr-in-rutile T estimates from graphite schist, although they show a larger spread of 726–854 °C (Table 1), overlap with the results from the pseudosection modelling.

The thermometer based on the isotopic equilibrium between carbonate and graphitic carbon gives additional support to the high-grade metamorphic conditions of graphite equilibration, where the $\delta^{13}C_{calcite}$ and $\delta^{13}C_{graphite}$ pairs indicate an equilibrium temperature ranging from 850 to 901 °C [58,59].

4.3. Role of Fluids

Graphite can originate by the metamorphism of organic deposited carbon; CO_2 fluxing and precipitation by decreasing carbon solubility, including fluid cooling [3]; water loss from mixed fluids during the hydrating reaction [4]; or the infiltration of fluid into a more reduced environment [5,73].

The importance of CO_2 fluid in orthopyroxene-bearing granulite facies metamorphism is well documented [18,20,74] and the formation of the anhydrous granulite has been explained by a massive CO_2 flux through the lower crust. Suggested sources of CO_2 include magmatic, mantle-derived, metamorphic decarbonitisation reactions or devolatilisation reactions in organic matter (e.g., [23]). The explanation of CO_2 infiltration is also controversial (e.g., [21]) and alternative explanations include dehydration by partial melting or the metamorphism of nearly dry rocks.

The $\delta^{13}C_{graphite}$ range of the graphite schists from Vesterålen studied here is consistent with the typical variation for Archean and Proterozoic organic deposited carbon, as discussed above. A reworking of carbon by later granulite-facies metamorphism can explain

the shift of the $\delta^{13}C_{graphite}$ to a heavier composition and the spread of the isotopic data (Table 2). This high-grade metamorphic overprint is further supported by the markedly heavier composition of the mixed graphite and calcite in samples SOM1701-59, SOM1701-60 and SOM1701-61 of $\delta^{13}C_{graphite}$ of −11.5 to −8.9, as a result of the exchange of isotopes between the graphite and calcite.

Although the carbon signature shows an organic deposited origin of the graphite, fluid mobility during high-grade metamorphism acts as an additional process in the petrogenesis of the high-ordered graphite. This coincides with [75], which described mixed metamorphic and fluid graphite deposition in Palaeoproterozoic sedimentary rocks of the Lewisian Complex. CO_2 infiltration may cause both orthopyroxene formation and graphite deposition. In our rocks, the intimate petrographic intergrowth of graphite with the minerals orthopyroxene, biotite, quartz and feldspar illustrates the relevance of the presence of CO_2 for the stabilisation of graphite in the orthopyroxene gneisses. The equilibration of graphite in granulite can occur via the following reaction:

$$\begin{gathered}2\ \text{Biotite} + 6\ \text{quartz} + CO_2 \Rightarrow 3\ \text{orthopyroxene} + 2\ \text{K-feldspar} + \text{graphite} + 2\ H_2O + O_2 \\ 2\ K(FeMg)_3AlSi_3O_{10}(OH)_2 + 6\ SiO_2 + CO_2 \Rightarrow 3\ (FeMg)_2Si_2O_6 + 2\ KAlSi_3O_8 + C + 2\ H_2O + O_2\end{gathered} \quad (1)$$

The release of H_2O is also a redox reaction (reducing CO_2), depositing graphite by releasing O_2. In a reduced environment, graphite can precipitate directly from CO_2 (e.g., [4]). This is possible if the rock mineral assemblage buffers fO_2 (e.g., [73]), and coincides with the presence of pyrrhotite, pyrite and chalcopyrite in the graphite schist (Figure 5; [5,76]).

Although regional CO_2 flux through the lower crust has been argued by [18,20,74], the close spatial occurrence of carbonate with the graphite schist in the Vestrålen complex may have acted as a CO_2 source during high-grade metamorphism, producing the observed clinopyroxene and olivine/forsterite as calcsilicate minerals:

$$\begin{gathered}\text{Dolomite} + 2\ SiO_2 \Rightarrow \text{Clinopyroxene/diopside} + 2\ CO_2 \\ CaMg(CO_3)_2 + 2\ SiO_2 \Rightarrow CaMgSi_2O_6 + 2\ CO_2\end{gathered} \quad (2)$$

$$\begin{gathered}2\ \text{Dolomite} + SiO_2 + O_2 \Rightarrow \text{olivine/forsterite} + 2\ \text{calcite} + 2\ CO_2 \\ 2\ CaMg(CO_3)_2 + SiO_2 + O_2 \Rightarrow Mg_2SiO_4 + 2\ CaCO_3 + 2\ CO_2\end{gathered} \quad (3)$$

The signature of CO_2 presence is also evident from the occurrence of meionitic (CO_2-bearing) scapolite ($Me_{74–81}$). The importance of redox reactions for graphite deposition is illustrated by the contemporaneous occurrence of graphite within sulphide-rich horizons (Figures 2c,d and 5d), a situation which is also documented by Parnell et al. [75]:

$$\begin{gathered}\text{Dolomite} + 2\ \text{Quartz} \Rightarrow \text{Clinopyroxene/diopside} + 2\ \text{graphite} + 2\ O_2 \\ CaMg(CO_3)_2 + 2\ SiO_2 \Rightarrow CaMgSi_2O_6 + 2\ C + 2\ O_2\end{gathered} \quad (4)$$

$$\begin{gathered}2\ \text{Dolomite} + \text{Quartz} \Rightarrow \text{olivine/forsterite} + 2\ \text{calcite} + 2\ \text{graphite} + O_2 \\ 2\ CaMg(CO_3)_2 + SiO_2 \Rightarrow Mg_2SiO_4 + 2\ CaCO_3 + 2\ C + O_2\end{gathered} \quad (5)$$

The intimate intergrowths of graphite with dolomite, calcite and forsterite/serpentine illustrate the relevance of the reactions above (samples VAE167, SOM1701-30.63, SOM1701-33.7 and SOM1701-45; Figure 4h). The contribution of SiO_2 to form calcsilicate minerals can alternatively be sourced from the original impure carbonate.

Additional evidence of the fluid effect on graphite deposition is the local high Mg# of biotite and pyroxenes in the graphite-bearing zones (Tables S2 and S4; Figure 5a–c). The increased Mg# values indicate metasomatism [77,78] related to graphite deposition. Furthermore, the same zones show an enrichment in Cl and F evidenced by their high content of apatite (Table S8; Figure 5d). High Cl content is an additional fluid flow tracer, as documented by Kullerud [35,79] from the AMCG suite of the neighbouring Lofoten–Vesterålen Complex, where Cl acts as an active ligand, enhancing element transport (e.g., [79–81]).

5. Conclusions

In this study, we document metamorphic graphite in Proterozoic granulite facies terrane of the Lofoten–Vesterålen Complex (north Norway), in addition to discussing its characterisation, origin, petrogenesis and the role of fluids:

- High-ordered graphite occurs in assemblage with metamorphic orthopyroxene in granulite-facies gneisses. Pseudosection modelling of the graphite + orthopyroxene (Mg# = 0.74) + plagioclase + biotite + quartz + rutile + ilmenite assemblage constrains its stability field to pressure–temperature conditions of 810–835 °C and 0.73–0.77 GPa. Zr-in-rutile supports a temperature of formation of 726–854 °C, while thermometry based on the isotopic equilibrium between carbonate and graphitic carbon gives additional support to the high-grade metamorphic conditions ranging from 850 to 900 °C.
- The graphite schist is hosted in sequences of banded orthopyroxene gneisses interlayered with horizons of marble, calcsilicate rocks and amphibolite. Graphite (modality < 39%) occurs in an assemblage with quartz, plagioclase ($Ab_{47–93}An_{5–52}$), orthopyroxene ($En_{69–74}Fs_{26–29}$; Mg# = 0.70–0.74), clinopyroxene ($En_{33–53}Fs_{1–14}Wo_{44–53}$; Mg# = 0.70–0.97), biotite (Mg# = 0.67–0.91; Ti < 0.66 a.p.f.u.) and K-feldspar ($Ab_{1–8}Kfs_{92–99}$) or perthite ($Ab_{35–64}An_3Kfs_{50–62}$), in addition to local epidote, clinozoisite, scapolite ($Me_{36–37}$; S = 0.05–0.07 a.p.f.u.; Cl = 0.66 a.p.f.u), white mica and garnet ($Alm_{16}Prp_{47–48}Grs_5Sps_{31–32}$). Graphite schist is enriched in sulphides (pyrite, pyrrhotite and chalcopyrite) with additional accessories of apatite, rutile, titanite and ilmenite.
- Stable C and O isotopes indicate an organic origin of graphite but with overprinting signatures of metamorphic and hydrothermal processes. Stable C isotopes support a source of organic carbon accumulated in sediments contemporaneous with the Early Proterozoic global Lomagundi–Jatuli isotopic excursion; the $\delta^{13}C_{graphite}$ of graphite schist is −38 to −17‰, while $\delta^{13}C_{calcite}$ values of marbles range from +3‰ to +10‰. Mixed graphitic and calcite carbon samples give lighter values for the calcite ($\delta^{13}C_{calcite}$ = −8.7‰ to −9.5‰) and heavier values for graphite ($\delta^{13}C_{grapite}$ = −11.5‰ to −8.9‰), indicating isotopic exchange between graphite and calcite during high-grade metamorphism. The $\delta^{18}O_{calcite}$ of marble shows relatively light values ranging from −15.4‰ to −7.5‰, possibly reflecting re-equilibration by metamorphic and fluid processes.
- The proposed mineral reaction equations illustrate the production and consumption of COH fluids, leading to the stabilisation of graphite, orthopyroxene, carbonate and silicate minerals during high-grade metamorphism.
- The high Mg# ratio of biotite and pyroxenes, together with a high Cl-F content of apatite (Cl < 2 a.p.f.u.; F < 1.44 a.p.f.u), supports the importance of fluid transport during the high-grade re-equilibration of graphite.

Supplementary Materials: The following supporting information can be downloaded at https://www.mdpi.com/article/10.3390/min13101279/s1: Table S1: Key localities and samples for petrography of graphite schist and related rocks (abbreviations after Whitney and Evans [53]). Table S2: Representative chemical data of pyroxenes; Table S3: Representative chemical data of feldspars; Table S4: Representative chemical data of sheet silicates; Table S5: Representative chemical data of amphibole; Table S6: Representative chemical data of garnet; Table S7: Representative chemical data of scapolite; Table S8: Representative chemical data of apatite; Table S9: Whole rock major elements (wt%) for pseudosection modelling; Table S10: TC and TOC (wt%) for pseudosection modelling.

Author Contributions: Conceptualisation, A.K.E., H.G. and M.E.; methodology, P.T.M. and J.K.S.; software, A.K.E.; validation, A.K.E., H.G. and M.E.; formal analysis, P.T.M. and M.E.; investigation, data curation, A.K.E., H.G., J.K.S., M.E. and P.T.M.; writing—original draft preparation, A.K.E.; writing—review and editing, H.G., M.E., P.T.M. and J.K.S. All authors have read and agreed to the published version of the manuscript.

Funding: The work was supported by the Geological Survey of Norway and received financial support from NGU-project 370800 from Nordland County Council.

Data Availability Statement: Data are available upon request.

Acknowledgments: Stable isotope analyses were carried out at the Norwegian National Infrastructure project FARLAB (Facility for Advanced Isotopic Research and Monitoring of Weather, Climate, and Biogeochemical Cycling, Project Nr. 245907) at the University of Bergen. We thank Aivo Lepland and Håkon Austrheim for fruitful discussions and three anonymous reviewers for their helpful comments.

Conflicts of Interest: There are no conflict of interest.

References

1. Buseck, P.R.; Beyssac, O. From Organic Matter to Graphite: Graphitization. *Elements* **2014**, *10*, 421–426. [CrossRef]
2. Case, G.N.D.; Karl, S.M.; Regan, S.P.; Johnson, C.A.; Ellison, E.T.; Caine, J.S.; Holm-Denoma, C.S.; Pianowski, L.S.; Marsh, J.H. Insights into the metamorphic history and origin of flake graphite mineralization at the Graphite Creek graphite deposit, Seward Peninsula, Alaska, USA. *Miner. Depos.* **2023**, *58*, 939–962. [CrossRef]
3. Rumble, D. Hydrothermal graphitic carbon. *Elements* **2014**, *10*, 427–433. [CrossRef]
4. Luque, F.; Huizenga, J.; Crespo-Feo, E.; Wada, H.; Ortega, L.; Barrenechea, J. Vein graphite deposits: Geological settings, origin, and economic significance. *Miner. Depos.* **2014**, *49*, 261–277. [CrossRef]
5. Touret, J.L.R.; Huizenga, J.M.; Kehelpannala, K.V.W.; Piccoli, F. Vein-type graphite deposits in Sri Lanka: The ultimate fate of granulite fluids. *Chem. Geol.* **2019**, *508*, 167–181. [CrossRef]
6. Santosh, M.; Wada, H. Microscale isotopic zonation in graphite crystals: Evidence for channelled CO influx in granulites. *Earth Planet. Sci. Lett.* **1993**, *119*, 19–26. [CrossRef]
7. Boyd, R.; Nordgulen, Ø.; Thomas, R.J.; Bingen, B.; Bjerkgård, T.; Grenne, T.; Henderson, I.; Melezhik, V.A.; Often, M.; Sandstad, J.S.; et al. The geology and geochemistry of the East African orogen in North eastern Mosambique. *S. Afr. J. Geol.* **2010**, *113*, 87–129. [CrossRef]
8. Collins, A.S.; Kinny, P.D.; Razakamanana, T. Depositional age, provenance and metamorphic age of metasedimentary rocks from southern Madagascar. *Gondwana Res.* **2012**, *21*, 353–361. [CrossRef]
9. Rosing-Schow, N.; Bagas, L.; Kolb, J.; Balić-Žunić, T.; Korte, C.; Fiorentini, M.L. Hydrothermal flake graphite mineralisation in Paleoproterozoic rocks of south-east Greenland. *Miner. Depos.* **2017**, *52*, 769–789. [CrossRef]
10. Gautneb, H.; Athola, T.; Torbjörn, B.; Gonzales, Y.; Aanders, H.; Schciptsov, V.; Voytekhovsky, Y. Industrial Mineral map of the Fennoscandian shield. In Proceedings of the 12th Biennal SGA Meeting, Uppsala, Sweden 2013; pp. 1767–1770.
11. Palosaari, J.; Latonen, R.M.; Smått, J.H.; Raunio, S.; Eklund, O. The flake graphite prospect of Piippumäki—An example of a high-quality graphite occurrence in a retrograde metamorphic terrain in Finland. *Miner. Depos.* **2020**, *55*, 1647–1660. [CrossRef]
12. Al-Ani, T.; Leinonen, S.; Ahtola, T.; Salvador, D. High-Grade Flake Graphite Deposits in Metamorphic Schist Belt, Central Finland—Mineralogy and Beneficiation of Graphite for Lithium-Ion Battery Applications. *Minerals* **2020**, *10*, 680. [CrossRef]
13. Gautneb, H.; Tveten, E. The geology, exploration and characterisation of graphite deposits in the Jennestad area, Vesterålen, northern Norway. *Nor. Geol. Undersøkelse Bull.* **2000**, *436*, 67–74.
14. Palosaari, J.; Latonen, R.-M.; Smått, J.-H.; Blomqvist, R.; Eklund, O. High-quality flake graphite occurrences in a high-grade metamorphic region in Sortland, Vesterålen, northern Norway. *Nor. J. Geol.* **2016**, *96*, 19–26. [CrossRef]
15. Gautneb, H.; Rønning, J.S.; Engvik, A.K.; Henderson, I.H.C.; Larsen, B.E.; Solberg, J.K.; Ofstad, F.; Gellein, J.; Elvebakk, H.; Davidsen, B. The Graphite Occurrences of Northern Norway, a Review of Geology, Geophysics, and Resources. *Minerals* **2020**, *10*, 626. [CrossRef]
16. Gautneb, H.; Rønning, J.S.; Larsen, B.E. A step towards meeting battery raw material demand: The geology and exploration of graphite deposits, examples from northern Norway. *Geol. Soc. Lond. Spec. Publ.* **2022**, *526*, 251–265. [CrossRef]
17. Al-Ani, T.; Ahtola, T.; Cutts, K.; Torppa, A. Metamorphic evolution of graphite in the Paleoproterozoic Savo Schist Belt (SSB), Central Finland: Constraints from geothermetric modeling. *Ore Geol. Rev.* **2022**, *141*, 104672. [CrossRef]
18. Touret, J. Le facies granulite en Norvege Meridionale: II. Les inclusions fluides. *Lithos* **1971**, *4*, 423–436. [CrossRef]
19. Strauss, H.; Melezhik, V.A.; Lepland, A.; Fallick, A.E.; Hanski, E.J.; Filippov, M.M.; Deines, Y.E.; Illing, C.J.; Črne, A.E.; Brasier, A.T. 7.6 Enhanced Accumulation of Organic Matter: The Shunga Event. In *Reading the Archive of Earth's Oxygenation*; Melezhik, V., Prave, A.R., Hanski, E.J., Fallick, A.E., Lepland, A., Kump, L.R., Strauss, H., Eds.; Springer: Berlin/Heidelberg, Germany, 2013; pp. 1195–1273.
20. Newton, R.; Smith, J.; Windley, B. Carbonic metamorphism, granulites and crustal growth. *Nature* **1980**, *288*, 45–50. [CrossRef]
21. Lamb, W.; Valley, J. Metamorphism of reduced granulites in low-CO_2 vapour-free environment. *Nature* **1984**, *312*, 56–58. [CrossRef]
22. Newton, R.C. Charnockitic alteration: Evidence for CO_2 infiltration in granulite facies metamorphism. *J. Metamorph. Geol.* **1992**, *10*, 383–400. [CrossRef]

23. Santosh, M.; Omori, S. CO_2 flushing: A plate tectonic perspective. *Gondwana Res.* **2008**, *13*, 86–102. [CrossRef]
24. Touret, J.L.R.; Huizenga, J.M. Fluid-assisted granulite metamorphism: A continental journey. *Gondwana Res.* **2012**, *21*, 224–235. [CrossRef]
25. Luque, d.V.F.J.; Pasteris, J.D.; Wopenka, B.; Rodas, M.; Fernández Barrenechea, J.M. Natural fluid-deposited graphite: Mineralogical characteristics and mechanisms of formation. *Am. J. Sci.* **1998**, *298*, 471–498. [CrossRef]
26. Galvez, M.E.; Beyssac, O.; Martinez, I.; Benzerara, K.; Chaduteau, C.; Malvoisin, B.; Malavieille, J. Graphite formation by carbonate reduction during subduction. *Nat. Geosci.* **2013**, *6*, 473–477. [CrossRef]
27. Galvez, M.E.; Pubellier, M. How Do Subduction Zones Regulate the Carbon Cycle? In *Deep Carbon: Past to Present*; Orcutt, B.N., Daniel, I., Dasgupta, R., Eds.; Cambridge University Press: Cambridge, UK, 2019; pp. 276–312.
28. Luque, F.J.; Crespo-Feo, E.; Barrenechea, J.F.; Ortega, L. Carbon isotopes of graphite: Implications on fluid history. *Geosci. Front.* **2012**, *3*, 197–207. [CrossRef]
29. Tveten, E. Svolvær. Berggrunnskart Svolvær M 1:250 000. Geological Survey of Norway. 1978. Available online: https://openarchive.ngu.no/ngu-xmlui/handle/11250/2663386 (accessed on 3 May 2023).
30. Griffin, W.L.; Taylor, P.N.; Hakkinen, J.W.; Heier, K.S.; Iden, I.K.; Krogh, E.J.; Malm, O.; Olsen, K.I.; Ormaasen, D.E.; Tveten, E. Archaean and Proterozoic crustal evolution in Lofoten–Vesterålen, N Norway. *J. Geol. Soc.* **1978**, *135*, 629–647. [CrossRef]
31. Corfu, F. U–Pb Age, Setting and Tectonic Significance of the Anorthosite–Mangerite–Charnockite–Granite Suite, Lofoten–Vesterålen, Norway. *J. Petrol.* **2004**, *45*, 1799–1819. [CrossRef]
32. Corfu, F. Multistage metamorphic evolution and nature of the amphibolite–granulite facies transition in Lofoten–Vesterålen, Norway, revealed by U–Pb in accessory minerals. *Chem. Geol.* **2007**, *241*, 108–128. [CrossRef]
33. Davidsen, B.; Skår, Ø. Lofoten and Vesterålen: A Precambrian puzzle. In Proceedings of the Geologiska Föreningens Förhandlingar, Nordic Geological Winter Meeting Sweden, Uppsala, Sweden, 6–9 January 2004; pp. 20–21.
34. Corfu, F.; Andersen, T.; Gasser, D. The Scandinavian Caledonides: Main features, conceptual advances and critical questions. *Geol. Soc. Lond. Spec. Publ.* **2014**, *390*, 9–43. [CrossRef]
35. Markl, G.; Frost, B.R.; Bucher, K. The Origin of Anorthosites and Related Rocks from the Lofoten Islands, Northern Norway: I. Field Relations and Estimation of Intrinsic Variables. *J. Petrol.* **1998**, *39*, 1425–1452. [CrossRef]
36. Keilhau, B.M. Beretning om en geonostisk reise i Norlandene i 1855. *Nyt Mag. Naturvidenskaberne* **1855**, *11*, 1–34.
37. Baker, A.J.; Fallick, A.E. Heavy carbon in two-billion-year-old marbles from Lofoten-Vesterålen, Norway: Implications for the Precambrian carbon cycle. *Geochim. Et Cosmochim. Acta* **1989**, *53*, 1111–1115. [CrossRef]
38. Baker, A.J.; Fallick, A.E. Evidence for CO_2 infiltration in granulite facies marbles from Lofoten-Vesteralen, Norway. *Earth Planet. Sci. Lett.* **1988**, *91*, 132–140. [CrossRef]
39. Rønning, J.S.; Gautneb, H.; Larsen, B.E.; Baranval, V.C.; Davidsen, B.; Engvik, A.; Gellein, J.; Knežević, J.; Ofstad, F.; Ren, X.; et al. *Geophysical and Geological Investigations of Graphite Occurrences in Vesterålen, Northern Norway, in 2018 and 2019*; Geological Survey of Norway Report 2019.031; Geological Survey of Norway: Trondheim, Norway, 2019; pp. 1–212.
40. Pouchou, J.P.; Pichoir, F. Cameca PAP program. *La Rech. Aerosp.* **1984**, *3*, 167–192.
41. Luvizotto, G.L.; Zack, T.; Meyer, H.P.; Ludwig, T.; Triebold, S.; Kronz, A.; Münker, C.; Stockli, D.F.; Prowatke, S.; Klemme, S.; et al. Rutile crystals as potential trace element and isotope mineral standards for microanalysis. *Chem. Geol.* **2009**, *261*, 346–369. [CrossRef]
42. de Capitani, C.; Petrakakis, K. The computation of equilibrium assemblage diagrams with Theriak/Domino software. *Am. Mineral.* **2010**, *95*, 1006–1016. [CrossRef]
43. Holland, T.; Powell, R. An internally consistent thermodynamic data set for phases of petrological interest. *J. Metamorph. Geol.* **1998**, *16*, 309–343. [CrossRef]
44. Newton, R.; Charlu, T.; Kleppa, O. Thermochemistry of the high structural state plagioclases. *Geochim. Et Cosmochim. Acta* **1980**, *44*, 933–941. [CrossRef]
45. Baldwin, J.; Powell, R.; Brown, M.; Moraes, R.; Fuck, R. Modelling of mineral equilibria in ultrahigh-temperature metamorphic rocks from the Anápolis–Itauçu Complex, central Brazil. *J. Metamorph. Geol.* **2005**, *23*, 511–531. [CrossRef]
46. White, R.W.; Powell, R.; Holland, T.J.B. Progress relating to calculation of partial melting equilibria for metapelites. *J. Metamorph. Geol.* **2007**, *25*, 511–527. [CrossRef]
47. Holland, T.; Powell, R. Thermodynamics of order-disorder in minerals; I, Symmetric formalism applied to minerals of fixed composition. *Am. Mineral.* **1996**, *81*, 1413–1424. [CrossRef]
48. Green, E.; Holland, T.; Powell, R. An order-disorder model for omphacitic pyroxenes in the system jadeite-diopside-hedenbergite-acmite, with applications to eclogitic rocks. *Am. Mineral.* **2007**, *92*, 1181–1189. [CrossRef]
49. Rønning, J.S.; Larsen, B.E.; Elvebakk, H.; Gautneb, H.; Ofstad, F.; Knežević, J. *Geophysical Investigations of Graphite Occurrences in Bø and Øksnes Municipalities, Vesterålen, Nordland County, Northern Norway 2015–2016*; NGU Report 2017.014; Geological Survey of Norway: Trondheim, Norway, 2017; pp. 1–50.
50. Gautneb, H.; Knežević, J.; Johannesen, N.E.; Wanvik, J.E.; Engvik, A.; Davidsen, B.; Rønning, J.S. *Geological and ore Dressing Investigations of Graphite Occurrences in Bø, Sortland, Hadsel and Øksnes Municipalities, Vesterålen, Nordland County, Northern Norway 2015–2016*; NGU Report 2017.015; Geological Survey of Norway: Trondheim, Norway, 2017; pp. 1–70.

51. Rodionov, A.; Ofstad, F.; Stampolidis, A.; Tassis, G. *Helicopter-Borne Magnetic, Electromagnetic and Radiometric Geophysical Survey at Langøya in Vesterålen, Nordland*; NGU Report 2013.044; Geological Survey of Norway: Trondheim, Norway, 2013; pp. 1–26.
52. Engvik, A.K.; Gautneb, H.; Baranwal, V.C.; Rønning, J.-S.; Solberg, K.J.; Liu, Y.; Austrheim, H. The control of shear-zone development and electric conductivity by graphite in granulite: An example from the Proterozoic Lofoten-Vesterålen Complex of northern Norway. *Terra Nova* **2021**, *33*, 529–539. [CrossRef]
53. Whitney, D.L.; Evans, B.W. Abbreviations for names of rock-forming minerals. *Am. Mineral.* **2010**, *95*, 185–187. [CrossRef]
54. Rønning, J.S.; Gautneb, H.; Larsen, B.E.; Knežević, S.J.; Baranval, V.C.; Elvebakk, H.; Gellein, J.; Ofstad, F.; Brönner, M. *Geophysical and Geological Investigations of Graphite Occurrences in Vesterålen and Lofoten, Northern Norway 2017*; Geological Survey of Norway: Trondheim, Norway, 2018; pp. 1–180.
55. Kohn, M.J. A refined zirconium-in-rutile thermometer. *Am. Mineral.* **2020**, *105*, 963–971. [CrossRef]
56. Tomkins, H.S.; Powell, R.; Ellis, D.J. The pressure dependence of the zirconium-in-rutile thermometer. *J. Metamorph. Geol.* **2007**, *25*, 703–713. [CrossRef]
57. Watson, E.B.; Wark, D.A.; Thomas, J.B. Crystallization thermometers for zircon and rutile. *Contrib. Mineral. Petrol.* **2006**, *151*, 413–433. [CrossRef]
58. Dunn, S.; Valley, J. Calcite–graphite isotope thermometry: A test for polymetamorphism in marble, Tudor gabbro aureole, Ontario, Canada. *J. Metamorph. Geol.* **1992**, *10*, 487–501. [CrossRef]
59. Wada, H.; Suzuki, K. Carbon isotopic thermometry calibrated by dolomite-calcite solvus temperatures. *Geochim. Et Cosmochim. Acta* **1983**, *47*, 697–706. [CrossRef]
60. Schidlowski, M. Organic matter in sedimentary rocks: «The dust we tread upon was once alive». *Terra Cogn.* **1983**, *4*, 45–49.
61. Schidlowski, M. Carbon isotopes as biogeochemical recorders of life over 3.8 Ga of Earth history: Evolution of a concept. *Precambrian Res.* **2001**, *106*, 117–134. [CrossRef]
62. Paiste, K.; Lepland, A.; Zerkle, A.L.; Kirsimäe, K.; Kreitsmann, T.; Mänd, K.; Romashkin, A.E.; Rychanchik, D.V.; Prave, A.R. Identifying global vs. basinal controls on Paleoproterozoic organic carbon and sulfur isotope records. *Earth-Sci. Rev.* **2020**, *207*, 103230. [CrossRef]
63. Parnell, J.; Brolly, C.; Boyce, A.J. Graphite from Palaeoproterozoic enhanced carbon burial, and its metallogenic legacy. *Geol. Mag.* **2021**, *158*, 1711–1718. [CrossRef]
64. Melezhik, V.A.; Fallick, A.E. A widespread positive δ13Ccarb anomaly at around 2.33–2.06 Ga on the Fennoscandian Shield: A paradox? *Terra Nova* **1996**, *8*, 141–157. [CrossRef]
65. Melezhik, V.A.; Huhma, H.; Condon, D.J.; Fallick, A.E.; Whitehouse, M.J. Temporal constraints on the Paleoproterozoic Lomagundi-Jatuli carbon isotopic event. *Geology* **2007**, *35*, 655–658. [CrossRef]
66. Melezhik, V.A.; Filippov, M.M.; Romashkin, A.E. A giant Palaeoproterozoic deposit of shungite in NW Russia: Genesis and practical applications. *Ore Geol. Rev.* **2004**, *24*, 135–154. [CrossRef]
67. Griffin, W.L. 'On the eclogites of Norway'—65 years later. *Mineral. Mag.* **1987**, *51*, 333–343. [CrossRef]
68. Beyssac, O.; Goffé, B.; Chopin, C.; Rouzaud, J. Raman spectra of carbonaceous material in metasediments: A new geothermometer. *J. Metamorph. Geol.* **2002**, *20*, 859–871. [CrossRef]
69. Rantitsch, G.; Lämmerer, W.; Fisslthaler, E.; Mitsche, S.; Kaltenböck, H. On the discrimination of semi-graphite and graphite by Raman spectroscopy. *Int. J. Coal Geol.* **2016**, *159*, 48–56. [CrossRef]
70. Pasteris, J.D. In Situ Analysis in Geological Thin-Sections by Laser Raman Microprobe Spectroscopy: A Cautionary Note. *Appl. Spectrosc.* **1989**, *43*, 567–570. [CrossRef]
71. Rantitsch, G.; Linner, M. Graphitization during high-grade metamorphism in the southern Bohemian Massif. *Int. J. Coal Geol.* **2021**, *248*, 103864. [CrossRef]
72. Satish-Kumar, M. Graphite-bearing CO2-fluid inclusions in granulites: Insights on graphite precipitation and carbon isotope evolution. *Geochim. Et Cosmochim. Acta* **2005**, *69*, 3841–3856. [CrossRef]
73. Huizenga, J.M.; Touret, J.L. Granulites, CO2 and graphite. *Gondwana Res.* **2012**, *22*, 799–809. [CrossRef]
74. Harley, S.L. Extending our understanding of ultrahigh temperature crustal metamorphism. *J. Mineral. Petrol. Sci.* **2004**, *99*, 140–158. [CrossRef]
75. Parnell, J.; Brolly, C.; Boyce, A. Mixed metamorphic and fluid graphite deposition in Palaeoproterozoic supracrustal rocks of the Lewisian Complex, NW Scotland. *Terra Nova* **2021**, *33*, 541–550. [CrossRef]
76. Kirilova, M.; Toy, V.G.; Timms, N.; Halfpenny, A.; Menzies, C.; Craw, D.; Beyssac, O.; Sutherland, R.; Townend, J.; Boulton, C. Textural changes of graphitic carbon by tectonic and hydrothermal processes in an active plate boundary fault zone, Alpine Fault, New Zealand. *Geol. Soc. Lond. Spec. Publ.* **2018**, *453*, 205–223. [CrossRef]
77. Engvik, A.K.; Ihlen, P.M.; Austrheim, H. Characterisation of Na-metasomatism in the Sveconorwegian Bamble Sector of South Norway. *Geosci. Front.* **2014**, *5*, 659–672. [CrossRef]
78. Engvik, A.K.; Mezger, K.; Wortelkamp, S.; Bast, R.; Corfu, F.; Korneliussen, A.; Ihlen, P.; Bingen, B.; Austrheim, H. Metasomatism of gabbro—Mineral replacement and element mobilization during the Sveconorwegian metamorphic event. *J. Metamorph. Geol.* **2011**, *29*, 399–423. [CrossRef]
79. Kullerud, K. Chlorine-rich amphiboles: Interplay between amphibole composition and an evolving fluid. *Eur. J. Mineral.* **1996**, *8*, 355–370. [CrossRef]

80. Engvik, A.K.; Golla-Schindler, U.; Berndt, J.; Austrheim, H.; Putnis, A. Intragranular replacement of chlorapatite by hydroxy-fluor-apatite during metasomatism. *Lithos* **2009**, *112*, 236–246. [CrossRef]
81. Liebscher, A. Experimental Studies in Model Fluid Systems. *Rev. Mineral. Geochem.* **2007**, *65*, 15–47. [CrossRef]